

Clustering by Maximizing Mutual Information Across Views

Kien Do, Truyen Tran, Svetha Venkatesh

Applied Artificial Intelligence Institute (A2I2), Deakin University, Geelong, Australia

{k.do, truyen.tran, svetha.venkatesh}@deakin.edu.au

Abstract

We propose a novel framework for image clustering that incorporates joint representation learning and clustering. Our method consists of two heads that share the same backbone network - a “representation learning” head and a “clustering” head. The “representation learning” head captures fine-grained patterns of objects at the instance level which serve as clues for the “clustering” head to extract coarse-grain information that separates objects into clusters. The whole model is trained in an end-to-end manner by minimizing the weighted sum of two sample-oriented contrastive losses applied to the outputs of the two heads. To ensure that the contrastive loss corresponding to the “clustering” head is optimal, we introduce a novel critic function called “log-of-dot-product”. Extensive experimental results demonstrate that our method significantly outperforms state-of-the-art single-stage clustering methods across a variety of image datasets, improving over the best baseline by about 5-7% in accuracy on CIFAR10/20, STL10, and ImageNet-Dogs. Further, the “two-stage” variant of our method also achieves better results than baselines on three challenging ImageNet subsets.

1. Introduction

The explosion of unlabeled data, especially visual content in recent years has led to the growing demand for effective organization of these data into semantically distinct groups in an unsupervised manner. Such data clustering facilitates downstream machine learning and reasoning tasks. Since labels are unavailable, clustering algorithms are mainly based on the similarity between samples to predict the cluster assignment. However, common similarity metrics such as cosine similarity or (negative) Euclidean distance are ineffective when applied to high-dimensional data like images. Modern image clustering methods [7, 19, 20, 43, 46, 47], therefore, leverage deep neural networks (e.g., CNNs, RNNs) to transform high-dimensional data into low-dimensional representation vectors in the latent space and perform clustering in that space.

Ideally, a good clustering model assigns data to clusters to keep inter-group similarity low while maintaining high intra-group similarity. Most existing deep clustering methods do not satisfy both of these properties. For example, autoencoder-based clustering methods [21, 46, 48] often learn representations that capture too much information including distracting information like background or texture. This prevents them from computing proper similarity scores between samples at the cluster-level. Autoencoder-based methods have only been tested on simple image datasets like MNIST. Another class of methods [7, 19, 20] directly use cluster-assignment probabilities rather than representation vectors to compute the similarity between samples. These methods can only differentiate objects belonging to different clusters but not in the same cluster, hence, may incorrectly group distinct objects into the same cluster. This leads to low intra-group similarity.

To address the limitations of existing methods, we propose a novel framework for image clustering called Contrastive Representation Learning and Clustering (CRLC). CRLC consists of two heads sharing the same backbone network: a “representation learning” head (RL-head) that outputs a continuous feature vector, and a “clustering” head (C-head) that outputs a cluster-assignment probability vector. The RL-head computes the similarity between objects at the instance level while the C-head separates objects into different clusters. The backbone network serves as a medium for information transfer between the two heads, allowing the C-head to leverage discriminative fine-grained patterns captured by the RL-head to extract correct coarse-grained cluster-level patterns. Via the two heads, CRLC can effectively modulate the inter-cluster and intra-cluster similarities between samples. CRLC is trained in an end-to-end manner by minimizing a weighted sum of two sample-oriented contrastive losses w.r.t. the two heads. To ensure that the contrastive loss corresponding to the C-head leads to the tightest InfoNCE lower bound [35], we propose a novel critic called “log-of-dot-product” to be used in place of the conventional “dot-product” critic.

In our experiments, we show that CRLC significantly outperforms a wide range of state-of-the-art single-

stage clustering methods on five standard image clustering datasets including CIFAR10/20, STL10, ImageNet10/Dogs. The “two-stage” variant of CRLC also achieves better results than SCAN - a powerful two-stage clustering method on three challenging ImageNet subsets with 50, 100, and 200 classes. When some labeled data are provided, CRLC, with only a small change in its objective, can surpass many state-of-the-art semi-supervised learning algorithms by a large margin.

In summary, our main contributions are:

1. A novel framework for joint representation learning and clustering trained via two sample-oriented contrastive losses on feature and probability vectors;
2. An optimal critic for the contrastive loss on probability vectors; and,
3. Extensive experiments and ablation studies to validate our proposed method against baselines.

2. Preliminaries

2.1. Representation learning by maximizing mutual information across different views¹

Maximizing mutual information across different views (or ViewInfoMax for short) allows us to learn view-invariant representations that capture the semantic information of data important for downstream tasks (e.g., classification). This learning strategy is also the key factor behind recent successes in representation learning [18, 33, 39, 42].

Since direct computation of mutual information is difficult [29, 37], people usually maximize the variational lower bounds of mutual information instead. The most common lower bound is InfoNCE [35] whose formula is given by:

$$I(X, \tilde{X}) \geq I_{\text{InfoNCE}}(X, \tilde{X}) \quad (1)$$

$$\triangleq \mathbb{E}_{p(x_{1:M})p(\tilde{x}|x_1)} \left[\log \frac{e^{f(\tilde{x}, x_1)}}{\sum_{i=1}^M e^{f(\tilde{x}, x_i)}} \right] + \log M \quad (2)$$

$$= -\mathcal{L}_{\text{contrast}} + \log M \quad (3)$$

where X, \tilde{X} denote random variables from 2 different views. $x_{1:M}$ are M samples from p_X , \tilde{x} is a sample from $p_{\tilde{X}}$ associated with x_1 . (\tilde{x}, x_1) is called a “positive” pair and (\tilde{x}, x_i) ($i = 2, \dots, M$) are called “negative” pairs. $f(x, y)$ is a real value function called “critic” that characterizes the similarity between x and y . $\mathcal{L}_{\text{contrast}}$ is often known as the “contrastive loss” in other works [8, 39].

Since $\log \frac{e^{f(\tilde{x}, x_1)}}{\sum_{i=1}^M e^{f(\tilde{x}, x_i)}} \leq 0$, $I_{\text{InfoNCE}}(X, \tilde{X})$ is upper-bounded by $\log M$. It means that: i) the InfoNCE bound

¹Here, we use “views” as a generic term to indicate different transformations of the same data sample.

is very loose if $I(X, \tilde{X}) \gg \log M$, and ii) by increasing M , we can achieve a better bound. Despite being biased, $I_{\text{InfoNCE}}(X, \tilde{X})$ has much lower variance than other unbiased lower bounds of $I(X, \tilde{X})$ [35], which allows stable training of models.

Implementing the critic In practice, $f(\tilde{x}, x_i)$ is implemented as the scaled cosine similarity between the representations of \tilde{x} and x_i as follows:

$$f(\tilde{x}, x_i) = f(\tilde{z}, z_i) = \tilde{z}^\top z_i / \tau \quad (4)$$

where \tilde{z} and z_i are *unit-normed* representation vectors of \tilde{x} and x_i , respectively; $\|\tilde{z}\|_2 = \|z_i\|_2 = 1$. $\tau > 0$ is the “temperature” hyperparameter. Interestingly, f in Eq. 4 matches the theoretically optimal critic that leads to the tightest InfoNCE bound for unit-normed representation vectors (detailed explanation in Appdx. A.4)

In Eq. 4, we use $f(\tilde{z}, z_i)$ instead of $f(\tilde{x}, x_i)$ to emphasize that the critic f in this context is a function of representations. In regard to this, we rewrite the contrastive loss in Eq. 3 as follows:

$$\mathcal{L}_{\text{FC}} = \mathbb{E}_{p(x_{1:M})p(\tilde{x}|x_1)} \left[-\log \frac{e^{f(\tilde{z}, z_1)}}{\sum_{i=1}^M e^{f(\tilde{z}, z_i)}} \right] \quad (5)$$

$$= \mathbb{E}_{p(x_{1:M})p(\tilde{x}|x_1)} \left[\tilde{z}^\top z_1 / \tau - \log \sum_{i=1}^M \exp(\tilde{z}^\top z_i / \tau) \right] \quad (6)$$

where FC stands for “feature contrastive”.

3. Method

3.1. Clustering by maximizing mutual information across different views

In the clustering problem, we want to learn a parametric classifier s_θ that maps each unlabeled sample x_i to a cluster-assignment probability vector $q_i = (q_{i,1}, \dots, q_{i,C})$ (C is the number of clusters) whose component $q_{i,c}$ characterizes how likely x_i belongs to the cluster c ($c \in \{1, \dots, C\}$). Intuitively, we can consider q_i as a representation of x_i and use this vector to capture the cluster-level information in x_i by leveraging the “ViewInfoMax” idea discussed in Section 2.1. It leads to the following loss for clustering:

$$\mathcal{L}_{\text{cluster}} = \mathbb{E}_{p(x_{1:M})p(\tilde{x}|x_1)} \left[-\log \frac{e^{f(\tilde{q}, q_1)}}{\sum_{i=1}^M e^{f(\tilde{q}, q_i)}} \right] - \lambda H(\tilde{Q}_{\text{avg}}) \quad (7)$$

$$= \mathcal{L}_{\text{PC}} - \lambda H(\tilde{Q}_{\text{avg}}) \quad (8)$$

where $\lambda \geq 0$ is a coefficient; \tilde{q}, q_i are probability vectors associated with \tilde{x} and x_i , respectively. \mathcal{L}_{PC} is the *prob-*

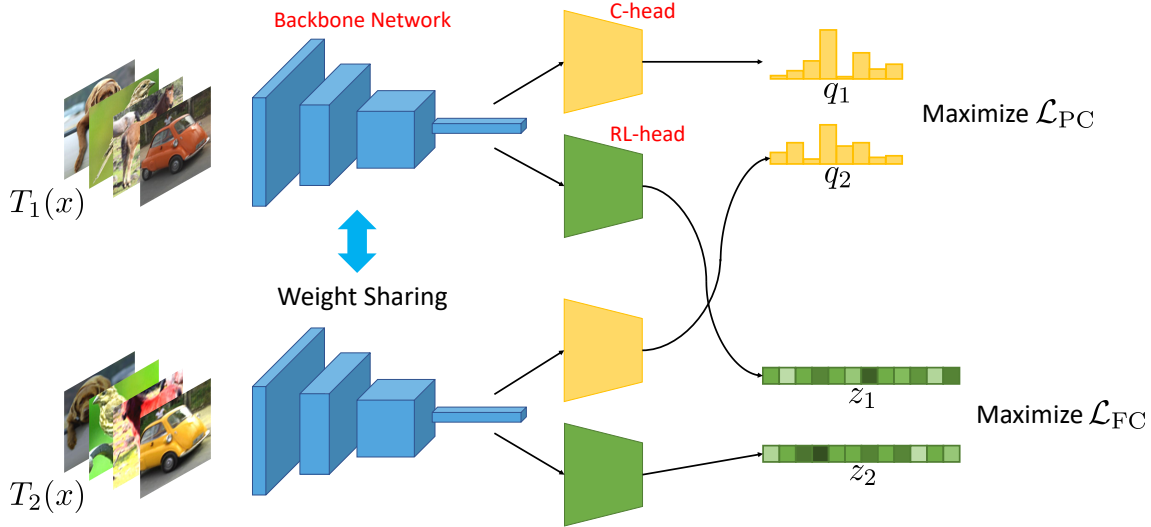


Figure 1: Overview of our proposed framework for Contrastive Representation Learning and Clustering (CRLC). Our framework consists of a “clustering” head and a “representation learning” head sharing the same backbone network. x denotes an input images and $T_1(x)$, $T_2(x)$ denote two different transformations of x .

bility contrastive loss similar to \mathcal{L}_{FC} (Eq. 5) but with feature vectors replaced by probability vectors. H is the entropy of the marginal cluster-assignment probability $\tilde{q}_{\text{avg}} = \mathbb{E}_{p(x_1)p(\tilde{x}|x_1)}[\tilde{q}]$. Here, we maximize $H(\tilde{Q}_{\text{avg}})$ to avoid a degenerate solution in which all samples fall into the same cluster (e.g., \tilde{q} is one-hot for all samples). However, it is free to use other regularizers on \tilde{q}_{avg} rather than $-H(\tilde{Q}_{\text{avg}})$.

Choosing a suitable critic It is possible to use the conventional “dot-product” critic for \mathcal{L}_{PC} as for \mathcal{L}_{FC} (Eq. 4). However, this will lead to suboptimal results (Section 5.3) since \mathcal{L}_{PC} is applied to categorical probability vectors rather than continuous feature vectors. Therefore, we need to choose a suitable critic for \mathcal{L}_{PC} so that the InfoNCE bound associated with \mathcal{L}_{PC} is tightest. Ideally, $f(\tilde{x}, x_i)$ should match the theoretically optimal critic $f^*(\tilde{x}, x_i)$ which is proportional to $\log p(\tilde{x}|x_i)$ (detailed explanation in Appdx. A.3). Denoted by \tilde{y} and y_i the cluster label of \tilde{x} and x_i respectively, we then have:

$$\begin{aligned} \log p(\tilde{x}|x_i) &\approx \log \sum_{c=1}^C p(\tilde{y} = c | y_i = c) \\ &\propto \log \sum_{c=1}^C \tilde{q}_c q_{i,c} = \log(\tilde{q}^\top q_i) \end{aligned} \quad (9)$$

Thus, the most suitable critic is $f(\tilde{q}, q_i) = \log(\tilde{q}^\top q_i)$ which we refer to as the “log-of-dot-product” critic. This critic achieves its maximum value when \tilde{q} and q_i are the same one-hot vectors and its minimum value when \tilde{q} and q_i are different one-hot vectors. Apart from this critic, we also list

other nonoptimal critics in Appdx. A.1. Empirical comparison of the “log-of-dot-product” critic with other critics is provided in Section 5.3.

In addition, to avoid the *gradient saturation* problem of minimizing \mathcal{L}_{PC} when probabilities are close to one-hot (explanation in Appdx. A.5), we smooth out the probabilities as follows:

$$q = (1 - \gamma)q + \gamma r$$

where $r = (\frac{1}{C}, \dots, \frac{1}{C})$ is the uniform probability vector over C classes; $0 \leq \gamma \leq 1$ is the smoothing coefficient set to 0.01 if not otherwise specified.

Implementing the contrastive probability loss To implement \mathcal{L}_{PC} , we can use either the SimCLR framework [8] or the MemoryBank framework [42]. If the SimCLR framework is chosen, both \tilde{q} and q_i ($i \in \{1, \dots, M\}$) are computed directly from \tilde{x} and x_i respectively via the parametric classifier s_θ . On the other hand, if the MemoryBank framework is chosen, we maintain a nonparametric memory bank \mathcal{M} - a matrix of size $N \times C$ containing the cluster-assignment probabilities of all N training samples, and update its rows once a new probability is computed as follows:

$$q_{n,t+1} = \alpha q_{n,t} + (1 - \alpha)\hat{q}_n \quad (10)$$

where α is the momentum, which is set to 0.5 in our work if not otherwise specified; $q_{n,t}$ is the probability vector of the training sample x_n at step t corresponding to the n -th row of \mathcal{M} ; $\hat{q}_n = s_\theta(x_n)$ is the new probability vector. Then, except \tilde{q} computed via s_θ as normal, all q_i in Eq. 7 are sampled uniformly from \mathcal{M} . At step 0, all the rows of \mathcal{M} are

initialized with the same probability of $(\frac{1}{C}, \dots, \frac{1}{C})$. We also tried implementing \mathcal{L}_{PC} using the MoCo framework [16] but found that it leads to unstable training. The main reason is that during the early stage of training, the EMA model in MoCo often produces inconsistent cluster-assignment probabilities for different views.

3.2. Incorporating representation learning

Due to the limited representation capability of categorical probability vectors, models trained by minimizing the loss $\mathcal{L}_{cluster}$ in Eq. 7 are not able to discriminate objects in the same cluster. Thus, they may capture suboptimal cluster-level patterns, which leads to unsatisfactory results.

To overcome this problem, we propose to combine clustering with contrastive representation learning into a unified framework called CRLC². As illustrated in Fig. 1, CRLC consists of a ‘‘clustering’’ head (C-head) and a ‘‘representation learning’’ head (RL-head) sharing the same backbone network. The backbone network is usually a convolutional neural network which maps an input image x into a hidden vector h . Then, h is fed to the C-head and the RL-head to produce a cluster-assignment probability vector q and a continuous feature vector z , respectively. We simultaneously apply the clustering loss $\mathcal{L}_{cluster}$ (Eq. 8) and the feature contrastive loss \mathcal{L}_{FC} (Eq. 6) on q and z respectively and train the whole model with the weighted sum of $\mathcal{L}_{cluster}$ and \mathcal{L}_{FC} as follows:

$$\begin{aligned} \mathcal{L}_{CRLC} &= \mathcal{L}_{cluster} + \lambda \mathcal{L}_{FC} \\ &= \mathcal{L}_{PC} - \lambda_1 H(\tilde{Q}_{avg}) + \lambda_2 \mathcal{L}_{FC} \end{aligned} \quad (11)$$

where $\lambda_1, \lambda_2 \geq 0$ are coefficients.

3.3. A simple extension to semi-supervised learning

Although CRLC is originally proposed for unsupervised clustering, it can be easily extended to semi-supervised learning (SSL). There are numerous ways to adjust CRLC so that it can incorporate labeled data during training. However, within the scope of this work, we only consider a simple approach which is adding a crossentropy loss on labeled data to \mathcal{L}_{CRLC} . The new loss is given by:

$$\begin{aligned} \mathcal{L}_{CRLC-semi} &= \mathcal{L}_{CRLC} + \lambda \mathbb{E}_{(x_l, y_l) \sim \mathcal{D}_l} [-\log p(y_l | x_l)] \\ &= \mathcal{L}_{PC} - \lambda_1 H(\tilde{Q}_{avg}) + \lambda_2 \mathcal{L}_{FC} + \lambda_3 \mathcal{L}_{xent} \end{aligned} \quad (12)$$

We call this variant of CRLC ‘‘CRLC-semi’’. Despite its simplicity, we will empirically show that CRLC-semi outperforms many state-of-the-art SSL methods when only few labeled samples are available. We conjecture that the clustering objective arranges the data into disjoint clusters, making classification easier.

²CRLC stands for Contrastive Representation Learning and Clustering.

4. Related Work

There are a large number of clustering and representation learning methods in literature. However, within the scope of this paper, we only discuss works in two related topics, namely, contrastive learning and deep clustering.

4.1. Contrastive Learning

Despite many recent successes in learning representations, the idea of contrastive learning appeared long time ago. In 2006, Hadsell et. al. [15] proposed a max-margin contrastive loss and linked it to a mechanical spring system. In fact, from a probabilistic view, contrastive learning arises naturally when working with energy-based models. For example, in many problems, we want to maximize $\log p(y|x) = \log \frac{e^{f(y,x)}}{\sum_{y' \in \mathcal{Y}} e^{f(y',x)}}$ where y is the output associated with a context x and \mathcal{Y} is the set of all possible outputs or vocab. This is roughly equivalent to maximizing $f(y, x)$ and minimizing $f(y', x)$ for all $y' \neq y$ but in a normalized setting. However, in practice, the size of \mathcal{Y} is usually very large, making the computation of $p(y|x)$ expensive. This problem was addressed in [32, 42] by using Noise Contrastive Estimation (NCE) [14] to approximate $p(y|x)$. The basic idea of NCE is to transform the density estimation problem into a binary classification problem: ‘‘Whether samples are drawn from the data distribution or from a known noise distribution?’’. Based on NCE, Mikolov et. al. [30] and Oord et. al. [33] derived a simpler contrastive loss which later was referred to as the InfoNCE loss [35] and was adopted by many subsequent works [8, 12, 16, 31, 39, 49] for learning representations.

Recently, there have been several attempts to leverage inter-sample statistics obtained from clustering to improve representation learning on a large scale [1, 4, 54]. PCL [26] alternates between clustering data via K-means and contrasting samples based on their views and their assigned cluster centroids (or prototypes). SwAV [5] does not contrast two sample views directly but uses one view to predict the code of assigning the other view to a set of learnable prototypes. InterCLR [44] and ODC [51] avoid offline clustering on the entire training dataset after each epoch by storing a pseudo-label for every sample in the memory bank (along with the feature vector) and maintaining a set of cluster centroids. These pseudo-labels and cluster centroids are updated on-the-fly at each step via mini-batch K-means.

4.2. Deep Clustering

Traditional clustering algorithms such as K-means or Gaussian Mixture Model (GMM) are mainly designed for low-dimensional vector-like data, hence, do not perform well on high-dimensional structural data like images. Deep clustering methods address this limitation by leveraging the representation power of deep neural networks (e.g., CNNs,

RNNs) to effectively transform data into low-dimensional feature vectors which are then used as inputs for a clustering objective. For example, DCN [46] applies K-means to the latent representations produced by an auto-encoder. The reconstruction loss and the K-means clustering loss are minimized simultaneously. DEC [43], by contrast, uses only an encoder rather than a full autoencoder like DCN to compute latent representations. This encoder and the cluster centroids are learned together via a clustering loss proposed by the authors. JULE [47] uses a RNN to implement agglomerative clustering on top of the representations outputted by a CNN and trains the two networks in an end-to-end manner. VaDE [21] regards clustering as an inference problem and learns the cluster-assignment probabilities of data using a variational framework [22]. Meanwhile, DAC [7] treats clustering as a binary classification problem: “Whether a pair of samples belong to the same cluster or not?”. To obtain a pseudo label for a pair, the cosine similarity between the cluster-assignment probabilities of the two samples in that pair is compared with an adaptive threshold. IIC [20] learns cluster assignments via maximizing the mutual information between clusters under two different data augmentations. PICA [19], instead, minimizes the contrastive loss derived from the the mutual information in IIC. While the cluster contrastive loss in PICA is cluster-oriented and can have at most C negative pairs (C is the number of clusters). Our probability contrastive loss, by contrast, is sample-oriented and can have as many negative pairs as the number of training data. Thus, in theory, our proposed model can capture more information than PICA. In real implementation, in order to gain more information from data, PICA has to make use of the “over-clustering” trick [20]. It alternates between minimizing $\mathcal{L}_{\text{PICA}}$ for C clusters and minimizing $\mathcal{L}_{\text{PICA}}$ for kC clusters ($k > 1$ denotes the “over-clustering” coefficient). DRC [53] and CC [27] enhances PICA by combining clustering with contrastive representation learning, which follows the same paradigm as our proposed CRLC. However, like PICA, DRC and CC uses cluster-oriented representations rather than sample-oriented representations.

In addition to end-to-end deep clustering methods, some multi-stage clustering methods have been proposed recently [34, 40]. The most notable one is SCAN [40]. This method uses representations learned via contrastive learning during the first stage to find nearest neighbors for every sample in the training set. In the second stage, neighboring samples are forced to have similar cluster-assignment probabilities. Our probability contrastive loss can easily be extended to handle neighboring samples (see Section 5.1.2).

5. Experiments

Dataset We evaluate our proposed method on 5 standard datasets for image clustering which are CIFAR10/20

[23], STL10 [9], ImageNet10 [11, 7], and ImageNet-Dogs [11, 7], and on 3 big ImageNet subsets namely ImageNet50/100/200 with 50/100/200 classes, respectively [11, 40]. A description of these datasets is given in Appdx. A.6. Our data augmentation setting follows [16, 42]. We first randomly crop images to a desirable size (32×32 for CIFAR, 96×96 for STL10, and 224×224 for ImageNet subsets). Then, we perform random horizontal flip, random color jittering, and random grayscale conversion. For datasets which are ImageNet subsets, we further apply Gaussian blurring at the last step [8]. Similar to previous works [7, 20, 19], both the training and test sets are used for CIFAR10, CIFAR20 and STL10 while only the training set is used for other datasets. We also provide results where only the training set is used for CIFAR10, CIFAR20 and STL10 in Appdx. A.8. For STL10, 100,000 auxiliary unlabeled samples are additionally used to train the “representation learning” head. However, when training the “clustering” head, these auxiliary samples are not used since their classes may not appear in the training set.

Model architecture and training setups Following previous works [19, 20, 40, 53], we adopt ResNet34 and ResNet50 [17] as the backbone network when working on the 5 standard datasets and on the 3 big ImageNet subsets, respectively. The “representation learning” head (RL-head) and the “clustering” head (C-head) are two-layer neural networks with ReLU activations. The length of the output vector of the RL-head is 128. The temperature τ (Eq. 5) is fixed at 0.1. To reduce variance in learning, we train our model with 10 C-subheads³ similar to [20]. This only adds little extra computation to our model. However, unlike [19, 20, 53], we do *not* use an auxiliary “over-clustering” head to exploit additional information from data since we think our RL-head can do that effectively.

Training setups for end-to-end and two-stage clustering are provided in Appdx. A.7.

Evaluation metrics We use three popular clustering metrics namely Accuracy (ACC), Normalized Mutual Information (NMI), Adjusted Rand Index (ARI) for evaluation. For unlabeled data, ACC is computed via the Kuhn-Munkres algorithm. All of these metrics scale from 0 to 1 and higher values indicate better performance. In this work, we convert the [0, 1] range into percentage.

5.1. Clustering

5.1.1 End-to-end training

Table 1 compares the performance of our proposed CRLC with a wide range of state-of-the-art deep clustering methods. CRLC clearly outperforms all baselines by a large

³The final $\mathcal{L}_{\text{cluster}}$ in Eq. 8 is the average of $\mathcal{L}_{\text{cluster}}$ of these C-subheads.

Dataset	CIFAR10			CIFAR20			STL10			ImageNet10			ImageNet-Dogs		
	ACC	NMI	ARI	ACC	NMI	ARI	ACC	NMI	ARI	ACC	NMI	ARI	ACC	NMI	ARI
JULE [47]	27.2	19.2	13.8	13.7	10.3	3.3	27.7	18.2	16.4	30.0	17.5	13.8	13.8	5.4	2.8
DEC [43]	30.1	25.7	16.1	18.5	13.6	5.0	35.9	27.6	18.6	38.1	28.2	20.3	19.5	12.2	7.9
DAC [7]	52.2	39.6	30.6	23.8	18.5	8.8	47.0	36.6	25.7	52.7	39.4	30.2	27.5	21.9	11.1
DDC [6]	52.4	42.4	32.9	-	-	-	48.9	37.1	26.7	57.7	43.3	34.5	-	-	-
DCCM [41]	62.3	49.6	40.8	32.7	28.5	17.3	48.2	37.6	26.2	70.1	60.8	55.5	38.3	32.1	18.2
IIC [20]	61.7	-	-	25.7	-	-	61.0	-	-	-	-	-	-	-	-
MCR2 [50]	68.4	63.0	50.8	34.7	36.2	16.7	49.1	44.6	29.0	-	-	-	-	-	-
PICA [19]	69.6	59.1	51.2	33.7	31.0	17.1	71.3	61.1	53.1	87.0	80.2	76.1	35.2	35.2	20.1
DRC [53]	72.7	62.1	54.7	36.7	35.6	20.8	74.7	64.4	56.9	88.4	83.0	79.8	38.9	38.4	23.3
C-head only	66.9	56.9	47.5	37.7	35.7	21.6	61.2	52.7	43.4	80.0	75.2	67.6	36.3	37.5	19.8
CRLC	79.9	67.9	63.4	42.5	41.6	26.3	81.8	72.9	68.2	85.4	83.1	75.9	46.1	48.4	29.7

Table 1: End-to-end clustering results on 5 standard image datasets. Due to space limit, we only show the means of the results. For the standard deviations, please refer to Appdx. A.8.

ImageNet	50 classes				100 classes				200 classes			
	ACC	ACC5	NMI	ARI	ACC	ACC5	NMI	ARI	ACC	ACC5	NMI	ARI
K-means [40]	65.9	-	77.5	57.9	59.7	-	76.1	50.8	52.5	-	75.5	43.2
SCAN [40]	75.1	91.9	80.5	63.5	66.2	88.1	78.7	54.4	56.3	80.3	75.7	44.1
two-stage CRLC	75.4	93.3	80.6	63.4	66.7	88.3	79.2	55.0	57.9	80.6	76.4	45.9

Table 2: Two-stage clustering results on ImageNet50/100/200.

margin on most datasets. For example, in term of clustering accuracy (ACC), our method improves over the best baseline (DRC [53]) by 5-7% on CIFAR10/20, STL10, and ImageNet-Dogs. Gains are even larger if we compare with methods that do not explicitly learn representations such as PICA [19] and IIC [20]. CRLC only performs worse than DRC on ImageNet10, which we attribute to our selection of hyperparameters. In addition, even when only the “clustering” head is used, our method still surpasses most of the baselines (e.g., DCCM, IIC). These results suggest that: i) we can learn semantic clusters from data just by minimizing the probability contrastive loss, and ii) combining with contrastive representation learning improves the quality of the cluster assignment.

To have a better insight into the performance of CRLC, we visualize some success and failure cases in Fig. 2 (and also in Appdx. A.11). We see that samples predicted correctly with high confidence are usually representative for the cluster they belong to. It suggests that CRLC has learned coarse-grained patterns that separate objects at the cluster level. Besides, CRLC has also captured fine-grained instance-level information, thus, is able to find nearest neighbors with great similarities in shape, color and texture to the original image. Another interesting thing from Fig. 2 is that the predicted label of a sample is often strongly correlated with that of the majority of its neighbors. It means

that: i) CRLC has learned a smooth mapping from images to cluster assignments, and ii) CRLC tends to make “collective” errors (the first and third rows in Fig. 2c). Other kinds of errors may come from the closeness between classes (e.g., horse vs. dog), or from some adversarial signals in the input (e.g., the second row in Fig. 2b). Solutions for fixing these errors are out of scope of this paper and will be left for future work.

5.1.2 Two-stage training

Although CRLC is originally proposed as an end-to-end clustering algorithm, it can be easily extended to a two-stage clustering algorithm similar to SCAN [40]. To do that, we first pretrain the RL-head and the backbone network with \mathcal{L}_{FC} (Eq. 6). Next, for every sample in the training data, we find a set of K nearest neighbors based on the cosine similarity between feature vectors produced by the pretrained network. In the second stage, we train the C-head by minimizing $\mathcal{L}_{cluster}$ (Eq. 8) with the positive pair consisting of a sample and its neighbor drawn from a set of K nearest neighbors. We call this variant of CRLC “two-stage” CRLC. In fact, we did try training both the C-head and the RL-head in the second stage by minimizing \mathcal{L}_{CRLC} but could not achieve good results compared to training only the C-head. We hypothesize that finetuning the RL-head causes the model to capture too much fine-grained informa-

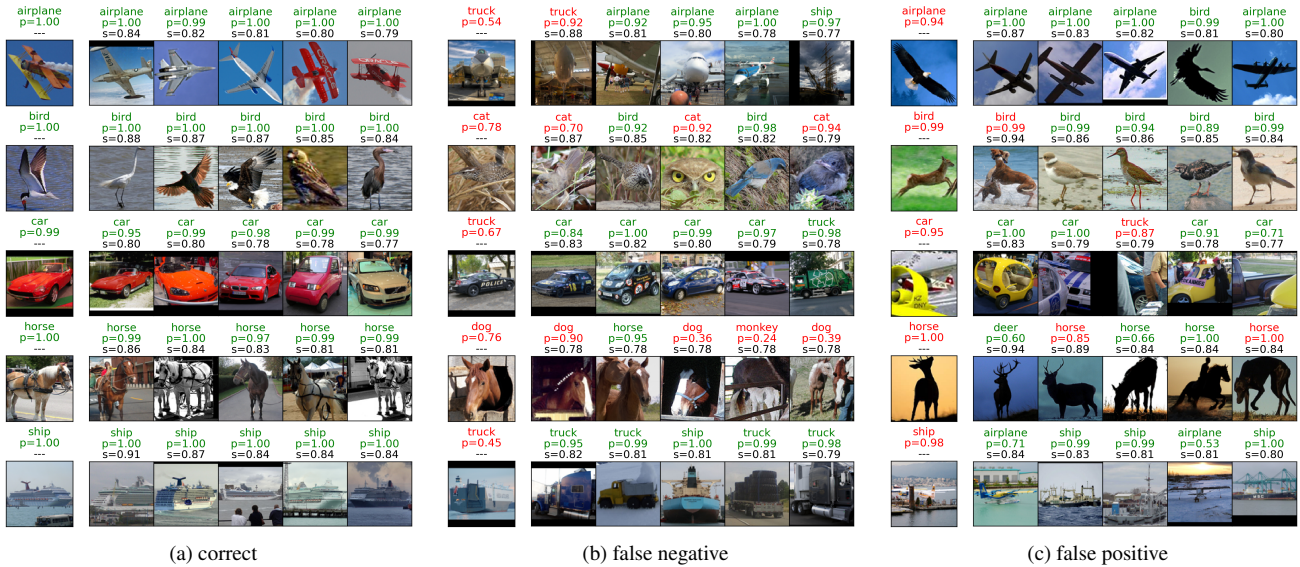


Figure 2: STL10 samples of 5 classes correctly (green) and incorrectly (red) predicted by CRLC. For each subplot, we show reference samples on the leftmost column and their nearest neighbors on the right. Neighbors are retrieved based on the normalized cosine similarity (“s”) between the feature vectors of two samples. “p” denotes the confidence probability.

Dataset	CIFAR10		
Labels	10	20	40
MixMatch [3]	-	-	47.54±11.50
UDA [45]	-	-	29.05±5.93
ReMixMatch [2]	-	-	19.10±9.64
ReMixMatch [†] [4]	59.86±9.34	41.68±8.15	28.31±6.72
CRLC-semi	46.75±8.01	29.81±1.18	19.87±0.82

Table 3: Classification errors on CIFAR10. Lower values are better. Results of baselines are taken from [36]. †: Results obtained from external implementations of models.

tion and ignore important cluster-level information, which hurts the clustering performance.

In Table 2, we show the clustering results of “two-stage” CRLC on ImageNet50/100/200. Results on CIFAR10/20 and STL10 are provided in Appdx. A.9. For fair comparison with SCAN, we use the same settings as in [40] (details in Appdx. A.7). It is clear that “two-stage” CRLC outperforms SCAN on all datasets. A possible reason is that besides pushing neighboring samples close together, our proposed probability contrastive loss also pulls away samples that are not neighbors (in the negative pairs) while the SCAN’s loss does not. Thus, by experiencing more pairs of samples, our model is likely to form better clusters.

⁴<https://github.com/google-research/remixmatch>

5.2. Semi-supervised Learning

Given the good performance of CRLC on clustering, it is natural to ask whether this model also performs well on semi-supervised learning (SSL) or not. To adapt for this new task, we simply train CRLC with the new objective $\mathcal{L}_{\text{CRLC-semi}}$ (Eq. 12). The model architecture and training setups remain almost the same (changes in Appdx. A.13).

From Table 3, we see that CRLC-semi, though is not designed especially for SSL, significantly outperforms many state-of-the-art SSL methods (brief discussion in Appdx. A.12). For example, CRLC-semi achieves about 30% and 10% lower error than MixMatch [3] and UDA [45] respectively on CIFAR10 with 4 labeled samples per class. Interestingly, the power of CRLC-semi becomes obvious when the number of labeled data is pushed to the limit. While most baselines cannot work with 1 or 2 labeled samples per class, CRLC-semi still performs *consistently well* with *very low standard deviations*. We hypothesize the reason is that CRLC-semi, via minimizing \mathcal{L}_{FC} , models the “smoothness” of data better than the SSL baselines. For more results on SSL, please check Appdx. A.14.

5.3. Ablation Study

Comparison of different critics in the probability contrastive loss In Fig. 3 left, we show the performance of CRLC on CIFAR10 and CIFAR20 w.r.t. different critic functions. Apparently, the theoretically sound “log-of-dot-product” critic (Eq. 9) gives the best results. The “negative-L2-distance” critic is slightly worse than the “log-of-dot-

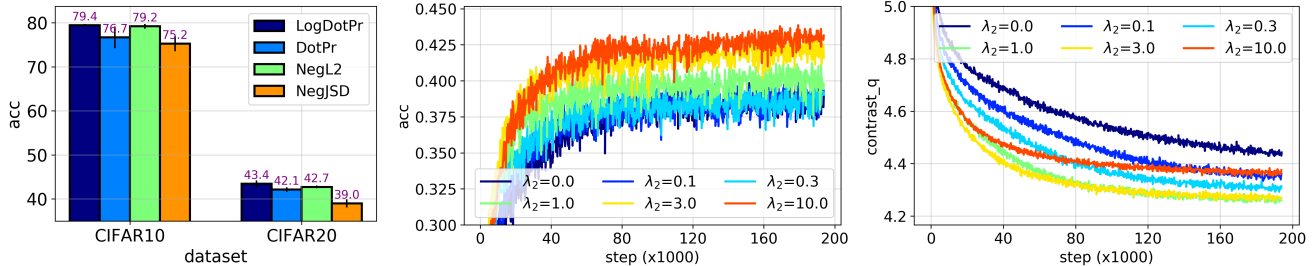


Figure 3: **Left:** Clustering accuracies of CRLC w.r.t. different critics on CIFAR10/20 (training set only). **Middle, Right:** Accuracy and \mathcal{L}_{PC} curves of CRLC on CIFAR20 w.r.t. different coefficients of \mathcal{L}_{FC} (λ_2 in Eq. 11).

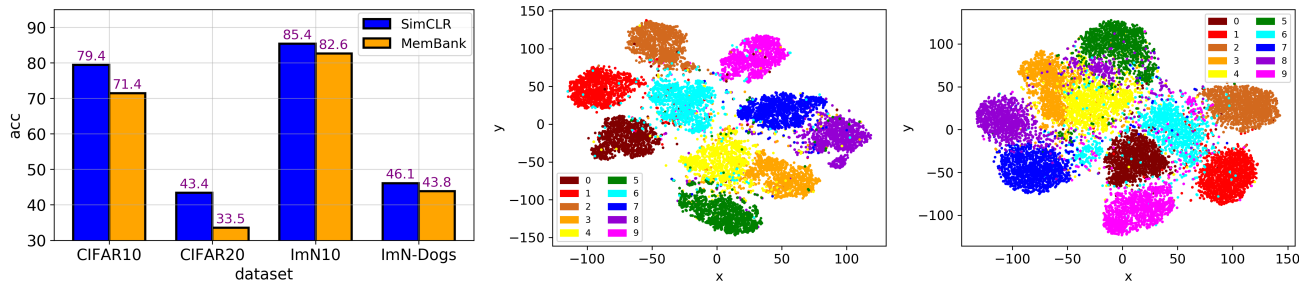


Figure 4: **Left:** Clustering accuracies of CRLC w.r.t. SimCLR [8] and MemoryBank [42] implementations. For CIFAR10/20, only the training set is used. **Middle, Right:** tSNE visualizations of the feature vectors learned by CRLC and SimCLR on the ImageNet10 train set, respectively.

product” critic while the “dot-product” and the “negative-JS-divergence” critics are the worst.

Contribution of the feature contrastive loss We investigate by how much our model’s performance will be affected if we change the coefficient of \mathcal{L}_{FC} (λ_2 in Eq. 11) to different values. Results on CIFAR20 are shown in Fig. 3 middle, right. Interestingly, minimizing both \mathcal{L}_{PC} and \mathcal{L}_{FC} simultaneously results in lower values of \mathcal{L}_{PC} than minimizing only \mathcal{L}_{PC} ($\lambda_2 = 0$). It implies that \mathcal{L}_{FC} provides the model with more information to form better clusters. In order to achieve good clustering results, λ_2 should be large enough relative to the coefficient of \mathcal{L}_{PC} which is 1. However, too large λ_2 results in a high value of \mathcal{L}_{PC} , which may hurt the model’s performance. For most datasets including CIFAR20, the optimal value of λ_2 is 10.

Nonparametric implementation of CRLC Besides using SimCLR [8], we can also implement the two contrastive losses in CRLC using MemoryBank [42] (Section 3.1). This reduces the memory storage by about 30% and the training time by half (on CIFAR10 with ResNet34 as the backbone and the minibatch size of 512). However, MemoryBank-based CRLC usually takes longer time to converge and is poorer than the SimCLR-based counterpart as shown in Fig. 4 left. The contributions of the number of negative samples and the momentum coefficient to the

performance of MemoryBank-based CRLC are analyzed in Appdx. A.10.2.

Mainfold visualization We visualize the manifold of the continuous features learned by CRLC in Fig. 4 middle. We observe that CRLC usually groups features into well-separated clusters. This is because the information captured by the C-head has affected the RL-head. However, if the RL-head is learned independently (e.g., in SimCLR), the clusters also emerge but are usually close together (Fig. 4 right). Through both cases, we see the importance of contrastive representation learning for clustering.

6. Conclusion

We proposed a novel clustering method named CRLC that exploits both the fine-grained instance-level information and the coarse-grained cluster-level information from data via a unified sample-oriented contrastive learning framework. CRLC showed promising results not only in clustering but also in semi-supervised learning. In the future, we plan to enhance CRLC so that it can handle neighboring samples in a principled way rather than just views. We also want to extend CRLC to other domains (e.g., videos, graphs) and problems (e.g., object detection).

References

- [1] Yuki Markus Asano, Christian Rupprecht, and Andrea Vedaldi. Self-labelling via simultaneous clustering and representation learning. *arXiv preprint arXiv:1911.05371*, 2019. [4](#)
- [2] David Berthelot, Nicholas Carlini, Ekin D Cubuk, Alex Kurakin, Kihyuk Sohn, Han Zhang, and Colin Raffel. Remixmatch: Semi-supervised learning with distribution alignment and augmentation anchoring. *arXiv preprint arXiv:1911.09785*, 2019. [7](#), [17](#), [18](#)
- [3] David Berthelot, Nicholas Carlini, Ian Goodfellow, Nicolas Papernot, Avital Oliver, and Colin A Raffel. Mixmatch: A holistic approach to semi-supervised learning. In *Advances in Neural Information Processing Systems*, pages 5050–5060, 2019. [7](#), [17](#), [18](#)
- [4] Mathilde Caron, Piotr Bojanowski, Armand Joulin, and Matthijs Douze. Deep clustering for unsupervised learning of visual features. In *Proceedings of the European Conference on Computer Vision (ECCV)*, pages 132–149, 2018. [4](#)
- [5] Mathilde Caron, Ishan Misra, Julien Mairal, Priya Goyal, Piotr Bojanowski, and Armand Joulin. Unsupervised learning of visual features by contrasting cluster assignments. *arXiv preprint arXiv:2006.09882*, 2020. [4](#)
- [6] Jianlong Chang, Yiwen Guo, Lingfeng Wang, Gaofeng Meng, Shiming Xiang, and Chunhong Pan. Deep discriminative clustering analysis. *arXiv preprint arXiv:1905.01681*, 2019. [6](#)
- [7] Jianlong Chang, Lingfeng Wang, Gaofeng Meng, Shiming Xiang, and Chunhong Pan. Deep adaptive image clustering. In *Proceedings of the IEEE international conference on computer vision*, pages 5879–5887, 2017. [1](#), [5](#), [6](#)
- [8] Ting Chen, Simon Kornblith, Mohammad Norouzi, and Geoffrey Hinton. A simple framework for contrastive learning of visual representations. *arXiv preprint arXiv:2002.05709*, 2020. [2](#), [3](#), [4](#), [5](#), [8](#), [13](#), [15](#)
- [9] Adam Coates, Andrew Ng, and Honglak Lee. An analysis of single-layer networks in unsupervised feature learning. In *Proceedings of the fourteenth international conference on artificial intelligence and statistics*, pages 215–223. JMLR Workshop and Conference Proceedings, 2011. [5](#)
- [10] Ekin D Cubuk, Barret Zoph, Jonathon Shlens, and Quoc V Le. Randaugment: Practical data augmentation with no separate search. *arXiv preprint arXiv:1909.13719*, 2019. [19](#)
- [11] Jia Deng, Wei Dong, Richard Socher, Li-Jia Li, Kai Li, and Li Fei-Fei. Imagenet: A large-scale hierarchical image database. In *2009 IEEE conference on computer vision and pattern recognition*, pages 248–255. Ieee, 2009. [5](#)
- [12] Alexey Dosovitskiy, Jost Tobias Springenberg, Martin Riedmiller, and Thomas Brox. Discriminative unsupervised feature learning with convolutional neural networks. In *Proceedings of the 27th International Conference on Neural Information Processing Systems-Volume 1*, pages 766–774, 2014. [4](#)
- [13] Prasoon Goyal, Zhiting Hu, Xiaodan Liang, Chenyu Wang, Eric P Xing, and Carnegie Mellon. Non-parametric variational auto-encoders for hierarchical representation learning. In *ICCV*, pages 5104–5112, 2017. [15](#)
- [14] Michael Gutmann and Aapo Hyvärinen. Noise-contrastive estimation: A new estimation principle for unnormalized statistical models. In *Proceedings of the Thirteenth International Conference on Artificial Intelligence and Statistics*, pages 297–304. JMLR Workshop and Conference Proceedings, 2010. [4](#)
- [15] Raia Hadsell, Sumit Chopra, and Yann LeCun. Dimensionality reduction by learning an invariant mapping. In *2006 IEEE Computer Society Conference on Computer Vision and Pattern Recognition (CVPR'06)*, volume 2, pages 1735–1742. IEEE, 2006. [4](#)
- [16] Kaiming He, Haoqi Fan, Yuxin Wu, Saining Xie, and Ross Girshick. Momentum contrast for unsupervised visual representation learning. In *Proceedings of the IEEE/CVF Conference on Computer Vision and Pattern Recognition*, pages 9729–9738, 2020. [4](#), [5](#), [15](#)
- [17] Kaiming He, Xiangyu Zhang, Shaoqing Ren, and Jian Sun. Deep residual learning for image recognition. In *Proceedings of the IEEE conference on computer vision and pattern recognition*, pages 770–778, 2016. [5](#)
- [18] R Devon Hjelm, Alex Fedorov, Samuel Lavoie-Marchildon, Karan Grewal, Phil Bachman, Adam Trischler, and Yoshua Bengio. Learning deep representations by mutual information estimation and maximization. *arXiv preprint arXiv:1808.06670*, 2018. [2](#)
- [19] Jiabo Huang, Shaogang Gong, and Xiatian Zhu. Deep semantic clustering by partition confidence maximization. In *Proceedings of the IEEE/CVF Conference on Computer Vision and Pattern Recognition*, pages 8849–8858, 2020. [1](#), [5](#), [6](#)
- [20] Xu Ji, João F Henriques, and Andrea Vedaldi. Invariant information clustering for unsupervised image classification and segmentation. In *Proceedings of the IEEE/CVF International Conference on Computer Vision*, pages 9865–9874, 2019. [1](#), [5](#), [6](#)

- [21] Zhuxi Jiang, Yin Zheng, Huachun Tan, Bangsheng Tang, and Hanning Zhou. Variational deep embedding: An unsupervised and generative approach to clustering. In *Proceedings of the 26th International Joint Conference on Artificial Intelligence*, pages 1965–1972, 2017. 1, 5
- [22] Diederik P Kingma and Max Welling. Auto-encoding variational bayes. *arXiv preprint arXiv:1312.6114*, 2013. 5
- [23] Alex Krizhevsky. Learning multiple layers of features from tiny images. 2009. 5
- [24] Samuli Laine and Timo Aila. Temporal ensembling for semi-supervised learning. *arXiv preprint arXiv:1610.02242*, 2016. 18
- [25] Dong-Hyun Lee. Pseudo-label: The simple and efficient semi-supervised learning method for deep neural networks. In *Workshop on challenges in representation learning, ICML*, volume 3, page 2, 2013. 18, 19
- [26] Junnan Li, Pan Zhou, Caiming Xiong, Richard Socher, and Steven CH Hoi. Prototypical contrastive learning of unsupervised representations. *arXiv preprint arXiv:2005.04966*, 2020. 4
- [27] Yunfan Li, Peng Hu, Zitao Liu, Dezhong Peng, Joey Tianyi Zhou, and Xi Peng. Contrastive clustering. *arXiv preprint arXiv:2009.09687*, 2020. 5
- [28] Ilya Loshchilov and Frank Hutter. SGDR: Stochastic gradient descent with warm restarts. *arXiv preprint arXiv:1608.03983*, 2016. 15, 17
- [29] David McAllester and Karl Stratos. Formal limitations on the measurement of mutual information. In *International Conference on Artificial Intelligence and Statistics*, pages 875–884. PMLR, 2020. 2
- [30] Tomas Mikolov, Ilya Sutskever, Kai Chen, Greg S Corrado, and Jeff Dean. Distributed representations of words and phrases and their compositionality. *Advances in Neural Information Processing Systems*, 26:3111–3119, 2013. 4
- [31] Ishan Misra and Laurens van der Maaten. Self-supervised learning of pretext-invariant representations. In *Proceedings of the IEEE/CVF Conference on Computer Vision and Pattern Recognition*, pages 6707–6717, 2020. 4
- [32] Andriy Mnih and Yee Whye Teh. A fast and simple algorithm for training neural probabilistic language models. In *Proceedings of the 29th International Conference on Machine Learning*, pages 419–426, 2012. 4
- [33] Aaron van den Oord, Yazhe Li, and Oriol Vinyals. Representation learning with contrastive predictive coding. *arXiv preprint arXiv:1807.03748*, 2018. 2, 4
- [34] Sungwon Park, Sungwon Han, Sundong Kim, Danu Kim, Sungkyu Park, Seunghoon Hong, and Meeyoung Cha. Improving unsupervised image clustering with robust learning. *arXiv preprint arXiv:2012.11150*, 2020. 5
- [35] Ben Poole, Sherjil Ozair, Aaron Van Den Oord, Alex Alemi, and George Tucker. On variational bounds of mutual information. In *International Conference on Machine Learning*, pages 5171–5180, 2019. 1, 2, 4, 12
- [36] Kihyuk Sohn, David Berthelot, Chun-Liang Li, Zizhao Zhang, Nicholas Carlini, Ekin D Cubuk, Alex Kurakin, Han Zhang, and Colin Raffel. Fixmatch: Simplifying semi-supervised learning with consistency and confidence. *arXiv preprint arXiv:2001.07685*, 2020. 7, 17, 18, 19
- [37] Jiaming Song and Stefano Ermon. Understanding the limitations of variational mutual information estimators. *arXiv preprint arXiv:1910.06222*, 2019. 2
- [38] Antti Tarvainen and Harri Valpola. Mean teachers are better role models: Weight-averaged consistency targets improve semi-supervised deep learning results. In *Advances in Neural Information Processing Systems*, pages 1195–1204, 2017. 18
- [39] Yonglong Tian, Dilip Krishnan, and Phillip Isola. Contrastive multiview coding. *arXiv preprint arXiv:1906.05849*, 2019. 2, 4, 15
- [40] Wouter Van Gansbeke, Simon Vandenhende, Stamatios Georgoulis, Marc Proesmans, and Luc Van Gool. Scan: Learning to classify images without labels. In *European Conference on Computer Vision*, pages 268–285. Springer, 2020. 5, 6, 7, 15, 16
- [41] Jianlong Wu, Keyu Long, Fei Wang, Chen Qian, Cheng Li, Zhouchen Lin, and Hongbin Zha. Deep comprehensive correlation mining for image clustering. In *Proceedings of the IEEE/CVF International Conference on Computer Vision*, pages 8150–8159, 2019. 6
- [42] Zhirong Wu, Yuanjun Xiong, Stella X Yu, and Dahua Lin. Unsupervised feature learning via non-parametric instance discrimination. In *Proceedings of the IEEE Conference on Computer Vision and Pattern Recognition*, pages 3733–3742, 2018. 2, 3, 4, 5, 8, 13
- [43] Junyuan Xie, Ross Girshick, and Ali Farhadi. Unsupervised deep embedding for clustering analysis. In *International conference on machine learning*, pages 478–487. PMLR, 2016. 1, 5, 6
- [44] Jiahao Xie, Xiaohang Zhan, Ziwei Liu, Yew Soon Ong, and Chen Change Loy. Delving into inter-image invariance for unsupervised visual representations. *arXiv preprint arXiv:2008.11702*, 2020. 4

- [45] Qizhe Xie, Zihang Dai, Eduard Hovy, Minh-Thang Luong, and Quoc V Le. Unsupervised data augmentation for consistency training. 2019. [7](#), [17](#), [18](#)
- [46] Bo Yang, Xiao Fu, Nicholas D Sidiropoulos, and Mingyi Hong. Towards k-means-friendly spaces: Simultaneous deep learning and clustering. In *international conference on machine learning*, pages 3861–3870. PMLR, 2017. [1](#), [5](#)
- [47] Jianwei Yang, Devi Parikh, and Dhruv Batra. Joint unsupervised learning of deep representations and image clusters. In *Proceedings of the IEEE conference on computer vision and pattern recognition*, pages 5147–5156, 2016. [1](#), [5](#), [6](#)
- [48] Linxiao Yang, Ngai-Man Cheung, Jiaying Li, and Jun Fang. Deep clustering by gaussian mixture variational autoencoders with graph embedding. In *Proceedings of the IEEE/CVF International Conference on Computer Vision*, pages 6440–6449, 2019. [1](#)
- [49] Mang Ye, Xu Zhang, Pong C Yuen, and Shih-Fu Chang. Unsupervised embedding learning via invariant and spreading instance feature. In *Proceedings of the IEEE/CVF Conference on Computer Vision and Pattern Recognition*, pages 6210–6219, 2019. [4](#)
- [50] Yaodong Yu, Kwan Ho Ryan Chan, Chong You, Chaobing Song, and Yi Ma. Learning diverse and discriminative representations via the principle of maximal coding rate reduction. *Advances in Neural Information Processing Systems*, 33, 2020. [6](#)
- [51] Xiaohang Zhan, Jiahao Xie, Ziwei Liu, Yew-Soon Ong, and Chen Change Loy. Online deep clustering for unsupervised representation learning. In *Proceedings of the IEEE/CVF Conference on Computer Vision and Pattern Recognition*, pages 6688–6697, 2020. [4](#)
- [52] Hongyi Zhang, Moustapha Cisse, Yann N Dauphin, and David Lopez-Paz. mixup: Beyond empirical risk minimization. *arXiv preprint arXiv:1710.09412*, 2017. [17](#)
- [53] Huasong Zhong, Chong Chen, Zhongming Jin, and Xian-Sheng Hua. Deep robust clustering by contrastive learning. *arXiv preprint arXiv:2008.03030*, 2020. [5](#), [6](#)
- [54] Chengxu Zhuang, Alex Lin Zhai, and Daniel Yamins. Local aggregation for unsupervised learning of visual embeddings. In *Proceedings of the IEEE/CVF International Conference on Computer Vision*, pages 6002–6012, 2019. [4](#)

A. Appendix

A.1. Possible critics for the probability contrastive loss

We list here several possible critics that could be used in \mathcal{L}_{PC} . If we simply consider a critic f as a similarity measure of two probabilities p and q , f could be the *negative Jensen Shannon (JS) divergence*⁵ between p and q :

$$\begin{aligned} f(p, q) &= -D_{\text{JS}}(p\|q) & (13) \\ &= -\frac{1}{2} \left(D_{\text{KL}} \left(p \left\| \frac{p+q}{2} \right. \right) + D_{\text{KL}} \left(q \left\| \frac{p+q}{2} \right. \right) \right) & (14) \end{aligned}$$

or the *negative L2 distance* between p and q :

$$f(p, q) = -\|p - q\|_2^2 = -\sum_{c=1}^C (p_c - q_c)^2 \quad (15)$$

In both cases, f achieves its maximum value when $p = q$ and its minimum value when p and q are different one-hot vectors.

We can also define f as the *dot product* of p and q as follows:

$$f(p, q) = p^\top q = \sum_{c=1}^C p_c q_c \quad (16)$$

However, the maximum value of this critic is no longer obtained when $p = q$ but when p and q are *the same one-hot vector* (check Appdx. A.2 for details). It means that maximizing this critic encourages not only the consistency between p and q but also the confidence of p and q .

A.2. Global maxima and minima of the dot product critic for probabilities

Proposition 1. The dot product critic $f(p, q) = \sum_{c=1}^C p_c q_c$ achieves its global maximum value at 1 when p_c and q_c are *the same one-hot vector*, and its global minimum value at 0 when p_c and q_c are *different one-hot vector*.

Proof. Since $0 \leq p_c, q_c \leq 1$, we have $\sum_{c=1}^C p_c q_c \geq 0$. This minimum value is achieved when $p_c q_c = 0$ for all $c \in \{1, \dots, C\}$. And because $\sum_{c=1}^C p_c = \sum_{c=1}^C q_c = 1$, p_c and q_c must be different one-hot vectors.

In addition, we also have $\sum_{c=1}^C p_c q_c \leq \sum_{c=1}^C p_c = 1$. This maximum value is achieved when $p_c q_c = p_c$ or $p_c(q_c - 1) = 0$ for all $c \in \{1, \dots, C\}$, which means p_c and q_c must be the same one-hot vectors. \square

Since the gradient of $\sum_{c=1}^C p_c q_c$ w.r.t. q_c is proportional to p_c , if we fix p and only optimize q , maximizing

⁵The JS divergence is chosen due to its symmetry. The negative sign reflects the fact that f is a similarity measure instead of a divergence.

$\sum_{c=1}^C p_c q_c$ via gradient ascent will encourage q to be *one-hot* at the component k at which p_k is the *largest*. Similarly, minimizing $\sum_{c=1}^C p_c q_c$ via gradient descent will encourage q to be *one-hot* at the component k at which p_k is the *smallest*.

In case $p_1 = \dots = p_C = \frac{1}{C}$, all the components of q have similar gradients. Although it does not change the relative order between the components of q after update, it still push q towards the saddle point $(\frac{1}{C}, \dots, \frac{1}{C})$. However, chance that models get stuck at this saddle point is tiny unless we explicitly force it to happen (e.g., maximizing $H(q)$).

For better understanding of the optimization dynamics, we visualize the surface of $\sum_{c=1}^C p_c q_c$ with $C = 2$ in Fig. 5a. $\log \left(\sum_{c=1}^C p_c q_c \right)$ has the same global optimal values and surface as $\sum_{c=1}^C p_c q_c$

A.3. Derivation of the InfoNCE lower bound

The variational lower bound of $I(X; Y)$ can be computed as follows:

$$\begin{aligned} I(X; Y) &= \mathbb{E}_{p(x, y)} \left[\log \frac{p(x, y)}{p(x)p(y)} \right] \\ &= \mathbb{E}_{p(x, y)} \left[\log \frac{q_\theta(x, y)}{p(x)p(y)} \right] + D_{\text{KL}}(p(x, y) \| q_\theta(x, y)) \\ &\geq \mathbb{E}_{p(x, y)} \left[\log \frac{q_\theta(x, y)}{p(x)p(y)} \right] & (17) \end{aligned}$$

where $q_\theta(x, y)$ is the variational approximation of $p(x, y)$.

Following [35], we assume that $q_\theta(x, y)$ belongs to the energy-based variational family that uses a critic $f_\theta(x, y)$ and is scaled by the data density $p(x)p(y)$:

$$q_\theta(x, y) = \frac{p(x)p(y)e^{f_\theta(x, y)}}{\sum_{x, y} p(x)p(y)e^{f_\theta(x, y)}} = \frac{p(x)p(y)e^{f_\theta(x, y)}}{Z_\theta} \quad (18)$$

where $Z_\theta = \sum_{x, y} p(x)p(y)e^{f_\theta(x, y)} = \mathbb{E}_{p(x)p(y)} [e^{f_\theta(x, y)}]$ is the partition function which does not depend on x, y .

Since the optimal value of $q_\theta(x, y)$ is $q_\theta^*(x, y) = p(x, y)$, we have:

$$\begin{aligned} \frac{p(x)p(y)e^{f_\theta^*(x, y)}}{Z_\theta^*} &= p(x, y) \\ \Leftrightarrow f_\theta^*(x, y) &= \log Z_\theta^* + \log \frac{p(x, y)}{p(x)p(y)}, & (19) \end{aligned}$$

which means the optimal value of $f_\theta(x, y)$ is proportional to $\log \frac{p(x, y)}{p(x)p(y)}$.

Next, we will show that f_θ is the critic in the InfoNCE lower bound. We start by rewriting the lower bound in Eq. 17 using the formula of $q_\theta(x)$ in Eq. 18 as follows:

$$\begin{aligned} I(X; Y) &\geq \mathbb{E}_{p(x, y)} \left[\log \frac{e^{f_\theta(x, y)}}{Z_\theta} \right] \\ &= \mathbb{E}_{p(x, y)} [f_\theta(x, y)] - \log Z_\theta & (20) \end{aligned}$$

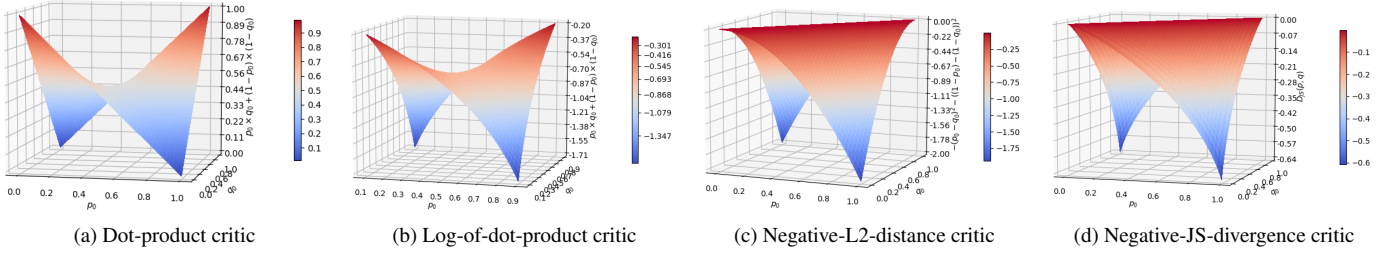


Figure 5: The surfaces of different critics on probabilities in case of 2 classes.

Here, we encounter the intractable $\log Z_\theta$. To form a tractable lower bound of $I(X; Y)$, we continue replacing $\log Z_\theta$ with its variational upper bound:

$$\log Z_\theta \leq \frac{Z_\theta}{a_\theta} + \log a_\theta - 1 \quad (21)$$

where a_θ is the variational approximation of Z_θ . We should choose a_θ close to Z_θ so that the variance of the bound in Eq. 21 is small. Recalling that $Z_\theta = \mathbb{E}_{p(x)p(y)} [e^{f_\theta(x,y)}]$, we define a_θ as follows:

$$a_\theta = \frac{1}{M} \sum_{i=1}^M e^{f_\theta(x_i, y)} \quad (22)$$

where x_1, \dots, x_M are M samples from $p(x)$. a_θ in Eq. 22 can be seen as a stochastic estimation of Z_θ with x sampled M times more than y . Thus, $\frac{Z_\theta}{a_\theta} \approx 1$ and from Eq. 21, we have $\log Z_\theta \leq \log a_\theta$. Apply this result to Eq. 20, we have:

$$I(X; Y) \geq \mathbb{E}_{p(x,y)} [f_\theta(x, y)] - \log a_\theta \quad (23)$$

$$= \mathbb{E}_{p(x_{2:M})} \mathbb{E}_{p(x_1, y)} \left[f_\theta(x_1, y) - \log \frac{1}{M} \sum_{i=1}^M e^{f_\theta(x_i, y)} \right] \quad (24)$$

$$= \mathbb{E}_{p(x_{1:M})p(y|x_1)} \left[\log \frac{e^{f_\theta(x_1, y)}}{\sum_{i=1}^M e^{f_\theta(x_i, y)}} \right] + \log M \quad (25)$$

$$\triangleq I_{\text{InfoNCE}}(X; Y) \quad (26)$$

where Eq. 24 is obtained from Eq. 23 by using the fact that $\mathbb{E}_{p(x,y)} [f_\theta(x, y)] = \mathbb{E}_{p(x_{2:M})} \mathbb{E}_{p(x_1, y)} [f_\theta(x_1, y)]$ and the assumption that the samples x_1, \dots, x_M and y in a_θ (Eq. 22) are drawn from $p(x_{2:M})p(x_1, y)$.

Combining with the result in Eq. 19, we have the optimal critic $f_\theta^*(x, y)$ in the InfoNCE lower bound is proportional to $\log \frac{p(x,y)}{p(x)p(y)} = \log \frac{p(y|x)}{p(y)}$. Since $p(y)$ does not depend on x and will be cancelled by both the nominator and denominator in Eq. 25, $f_\theta^*(x, y)$ is, in fact, proportional to $\log p(y|x)$.

A.4. Derivation of the scaled dot product critic in representation learning

Recalling that in contrastive representation learning, the critic f is defined as the scaled dot product between two unit-normed feature vectors \tilde{z}, z_i :

$$f(\tilde{x}, x_i) = \tilde{z}^\top z_i / \tau$$

Interestingly, this formula of f is accordant with the formula of f^* and is proportional to $\log p(\tilde{x}|x_i)$. To see why, let's assume that the distribution of \tilde{z} given z_i is modeled by an isotropic Gaussian distribution with z_i as the mean vector and τI as the covariance matrix. Then, we have:

$$\begin{aligned} f^* &\propto \log p(\tilde{x}|x_i) \\ &\approx \log p(\tilde{z}|z_i) \\ &\propto \log e^{-\frac{0.5}{\tau} \|\tilde{z} - z_i\|_2^2} \\ &= -\frac{0.5}{\tau} \left(\|\tilde{z}\|_2^2 - 2\tilde{z}^\top z_i + \|z_i\|_2^2 \right) \\ &= \tilde{z}^\top z_i / \tau - 1/\tau \\ &\propto \tilde{z}^\top z_i / \tau \end{aligned}$$

where $\|\tilde{z}\|_2^2 = \|z_i\|_2^2 = 1$ due to the fact that \tilde{z} and z_i are unit-normed vectors.

A.5. Analysis of the gradient of \mathcal{L}_{PC}

Recalling that the probability contrastive loss \mathcal{L}_{PC} for a sample \tilde{x} with the ‘‘log-of-dot-product’’ critic $f(p, q) = \log(p^\top q)$ is computed as follows:

$$\begin{aligned} \mathcal{L}_{\text{PC}} &= -\log \frac{e^{f(\tilde{q}, q_1)}}{\sum_{i=1}^M e^{f(\tilde{q}, q_i)}} \\ &= -\log(\tilde{q}^\top q_1) + \log \sum_{i=1}^M \tilde{q}^\top q_i \end{aligned}$$

Because \tilde{q} is always parametric while q_i ($i \in \{1, \dots, M\}$) can be either parametric (if \mathcal{L}_{PC} is implemented via the SimCLR framework [8]) or non-parametric (if \mathcal{L}_{PC} is implemented via the MemoryBank framework [42]), we focus

on the gradient of \mathcal{L}_{PC} back-propagating through \tilde{q} . In practice, \tilde{q} is usually implemented by applying softmax to the logit vector $\tilde{u} \in \mathbb{R}^C$:

$$\tilde{q}_c = \frac{\exp(\tilde{u}_c)}{\sum_{k=1}^C \exp(\tilde{u}_k)}$$

where \tilde{q}_c denotes the c -th component of \tilde{q} . Similarly, $q_{i,c}$ is the c -th component of q_i .

The gradient of \mathcal{L}_{PC} w.r.t. \tilde{u}_c is given by:

$$\frac{\partial \mathcal{L}_{\text{PC}}}{\partial \tilde{u}_c} = -\frac{\partial}{\partial \tilde{u}_c} \log(\tilde{q}^\top q_1) + \frac{\partial}{\partial \tilde{u}_c} \log \sum_{i=1}^M \tilde{q}^\top q_i \quad (27)$$

The first term in Eq. 27 is equivalent to:

$$\begin{aligned} & -\frac{\partial}{\partial \tilde{u}_c} \log(\tilde{q}^\top q_1) \\ \Leftrightarrow & \frac{-1}{\tilde{q}^\top q_1} \left(\frac{\partial}{\partial \tilde{u}_c} (\tilde{q}_c q_{1,c}) + \sum_{k \neq c} \frac{\partial}{\partial \tilde{u}_c} (\tilde{q}_k q_{1,k}) \right) \\ \Leftrightarrow & \frac{-1}{\tilde{q}^\top q_1} \left(\tilde{q}_c (1 - \tilde{q}_c) q_{1,c} - \sum_{k \neq c} \tilde{q}_k \tilde{q}_k q_{1,k} \right) \\ \Leftrightarrow & -\frac{1}{\sum_{k=1}^C \tilde{q}_k q_{1,k}} \left(\tilde{q}_c q_{1,c} - \tilde{q}_c \sum_{k=1}^C \tilde{q}_k q_{1,k} \right) \\ \Leftrightarrow & \tilde{q}_c - \frac{\tilde{q}_c q_{1,c}}{\sum_{k=1}^C \tilde{q}_k q_{1,k}} \end{aligned} \quad (28)$$

And the second term in Eq. 27 is equivalent to:

$$\begin{aligned} & \frac{\partial}{\partial \tilde{u}_c} \log \sum_{i=1}^M \tilde{q}^\top q_i \\ \Leftrightarrow & \frac{1}{\sum_{i=1}^M \tilde{q}^\top q_i} \left(\sum_{i=1}^M \frac{\partial}{\partial \tilde{u}_c} (\tilde{q}^\top q_i) \right) \\ \Leftrightarrow & \frac{1}{\sum_{i=1}^M \tilde{q}^\top q_i} \left(\sum_{i=1}^M \left(\tilde{q}_c q_{i,c} - \tilde{q}_c \sum_{k=1}^C \tilde{q}_k q_{i,k} \right) \right) \\ \Leftrightarrow & \frac{1}{\sum_{i=1}^M \sum_{k=1}^C \tilde{q}_k q_{i,k}} \left(\sum_{i=1}^M \tilde{q}_c q_{i,c} - \tilde{q}_c \sum_{i=1}^M \sum_{k=1}^C \tilde{q}_k q_{i,k} \right) \\ \Leftrightarrow & \frac{\sum_{i=1}^M \tilde{q}_c q_{i,c}}{\sum_{i=1}^M \sum_{k=1}^C \tilde{q}_k q_{i,k}} - \tilde{q}_c \end{aligned}$$

Thus, we have:

$$\frac{\partial \mathcal{L}_{\text{PC}}}{\partial \tilde{u}_c} = \frac{\sum_{i=1}^M \tilde{q}_c q_{i,c}}{\sum_{i=1}^M \sum_{k=1}^C \tilde{q}_k q_{i,k}} - \frac{\tilde{q}_c q_{1,c}}{\sum_{k=1}^C \tilde{q}_k q_{1,k}} \quad (29)$$

We care about the second term in Eq. 29 which is derived from the gradient of the critic $f(\tilde{q}, q_1)$ w.r.t. \tilde{u}_c (the negative of the term in Eq. 28). We rewrite this gradient with

Dataset	#Train	#Test	#Extra	#Classes	Image size
CIFAR10	50,000	10,000	×	10	32×32×3
CIFAR20	50,000	10,000	×	20	32×32×3
STL10	5,000	8,000	100,000	10	96×96×3
ImageNet10	13,000	500	×	10	224×224×3
ImageNet-Dogs	19,500	750	×	15	224×224×3
ImageNet-50	64,274	2,500	×	50	224×224×3
ImageNet-100	128,545	5,000	×	100	224×224×3
ImageNet-200	256,558	10,000	×	200	224×224×3

Table 4: Details of the datasets used in this work.

simplified notations as follows:

$$\frac{\partial f(q, p)}{\partial u_c} = \frac{q_c p_c}{\sum_{k=1}^C q_k p_k} - q_c$$

where u_c is the c -th logit of q . Since during training, q is encouraged to be one-hot (see Appdx. A.2), the denominator may not be defined if we do not prevent p from being a different one-hot vector. However, even when the denominator is defined, the update still does not happen as expected when q is one-hot. To see why, let's consider a simple scenario in which $q = [0, 1, 0]$ and $p = [0.998, 0.001, 0.001]$. Apparently, the denominator is $0.001 \neq 0$. By maximizing $f(q, p)$, we want to push q toward p . Thus, we expect that $\frac{\partial f}{\partial u_1} > 0$ and $\frac{\partial f}{\partial u_2} < 0$. However, the gradients w.r.t. u_c are 0s for all $c \in \{1, 2, 3\}$:

$$\begin{aligned} \frac{\partial f}{\partial u_1} &= \frac{0 \times 0.998}{0.001} - 0 = 0 \\ \frac{\partial f}{\partial u_2} &= \frac{1 \times 0.001}{0.001} - 1 = 0 \\ \frac{\partial f}{\partial u_3} &= \frac{0 \times 0.001}{0.001} - 0 = 0 \end{aligned}$$

The reason is that $q = [0, 1, 0]$ is a stationary point (minimum in this case). This means once the model has set q to be one-hot, it tends to get stuck there and cannot escape *regardless of the value of p* . This problem is known in literature as the ‘‘saturating gradient’’ problem. To alleviate this problem, we propose to smooth out the values of q and p before computing the critic f :

$$\begin{aligned} q &= (1 - \gamma)q + \gamma r \\ p &= (1 - \gamma)p + \gamma r \end{aligned}$$

where $0 \leq \gamma \leq 1$ is the smoothing coefficient, which is set to 0.01 if not otherwise specified; $r = (\frac{1}{C}, \dots, \frac{1}{C})$ is the uniform probability vector over classes. We also regularize the value of u_c to be within $[-25, 25]$.

Dataset		CIFAR10			CIFAR20			STL10		
Metric		ACC	NMI	ARI	ACC	NMI	ARI	ACC	NMI	ARI
C-head only	Train only	67.2±0.7	56.8±1.3	47.8±1.4	38.0±1.6	36.8±1.0	22.3±0.9	47.03±2.2	39.06±1.5	27.23±1.8
	Train + Test	66.9±0.8	56.9±0.7	47.5±0.5	37.7±0.4	35.7±0.5	21.6±0.3	61.2±1.2	52.7±0.8	43.4±1.3
CRLC	Train only	79.4±0.3	66.7±0.6	62.3±0.4	43.4±0.8	43.1±0.5	27.7±0.3	57.6±1.6	50.8±1.5	41.9±1.2
	Train + Test	79.9±0.6	67.9±0.6	63.4±0.4	42.5±0.7	41.6±0.8	26.3±0.5	81.8±0.3	72.9±0.4	68.2±0.3

Table 5: Clustering results of our proposed methods on CIFAR10, CIFAR20 and STL10 with only the training set used and with both the training and test sets used.

Dataset	ImageNet10			ImageNet-Dogs		
	ACC	NMI	ARI	ACC	NMI	ARI
C-head only	80.0±1.4	75.2±1.9	67.6±2.2	36.3±0.9	37.5±0.7	19.8±0.4
CRLC	85.4±0.3	83.1±0.5	75.9±0.4	46.1±0.6	48.4±0.6	29.7±0.4

Table 6: Clustering results of our proposed methods on ImageNet10 and ImageNet-Dogs.

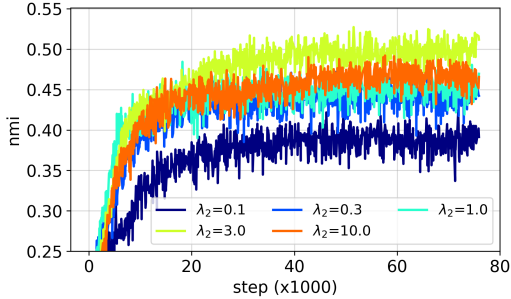


Figure 6: NMI curve of CRLC on ImageNet-Dogs w.r.t. different coefficients of \mathcal{L}_{FC} .

A.6. Dataset description

In Table 4, we provide details of the datasets used in this work. CIFAR20 is CIFAR100 with 100 classes replaced by 20 super-classes. STL10 is different from other datasets in the sense that it has an auxiliary set of 100,000 unlabeled samples of unknown classes. Similar to previous works, we use samples from this auxiliary set and the training set to train the “representation learning” head.

A.7. Training setups for clustering

End-to-end clustering For end-to-end clustering, we use a SGD optimizer with a constant learning rate = 0.1, momentum = 0.9, Nesterov = False, and weight decay = $5e-4$ based on the settings in [13, 16, 39]. We set the batch size to 512 and the number of epochs to 2000. In fact, on some datasets like ImageNet10 or ImageNet-Dogs, CRLC only needs 500 epochs to converge. The coefficients of the negative entropy and \mathcal{L}_{FC} (λ_1 and λ_2 in Eq. 11 in the main text) are fixed at 1 and 10, respectively. Each experiment is repeated 3 times with random initializations.

Two-stage clustering For two-stage clustering, we use the same settings as in [40]. Specifically, the backbone network is ResNet18 for CIFAR10/20, STL10 and is ResNet50 for ImageNet50/100/200. In the first (pretraining) stage, for CIFAR10/20 and STL10, we pretrain the backbone network and the RL-head via SimCLR [8] for 500 epochs. The optimizer is SGD with an initial learning rate = 0.4 decayed with a cosine decay schedule [28], momentum = 0.9, Nesterov = False, and weight decay = $1e-4$. Meanwhile, for ImageNet50/100/200, we directly copy the pretrained weights of MoCo [16] to the backbone network and the RL-head. After the pretraining stage, we find for each sample in the training set 50 nearest neighbors based on the cosine similarity measure. Positive samples for contrastive learning in the second stage are drawn uniformly from these sets of nearest neighbors. In the second stage, for CIFAR10/20 and STL10, we train both the backbone network and the C-head for 200 epochs by minimizing $\mathcal{L}_{cluster}$ (Eq. 8 in the main text) using an Adam optimizer with a constant learning rate = $1e-4$ and weight decay = $1e-4$. For ImageNet50/100/200, we freeze the backbone network and only train the C-head for 200 epochs by minimizing $\mathcal{L}_{cluster}$ using an SGD optimizer with a constant learning rate = 5.0, momentum = 0.9, Nesterov = False, and weight decay = 0.0.

A.8. Complete end-to-end clustering results

Complete results with standard deviations on the five standard clustering datasets are shown in Tables 5 and 6. From Table 5, we see that for CIFAR10 using both the training and test sets does not cause much difference in performance compared to using only the training set. For CIFAR20, using only the training set even leads to slightly better results. By contrast, for STL10, models trained with both the training and test sets significantly outperform those trained with the training set only. We believe the reason

Dataset	CIFAR10			CIFAR20			STL10		
	ACC	NMI	ARI	ACC	NMI	ARI	ACC	NMI	ARI
K-means [40]	65.9±5.7	59.8±2.0	50.9±3.7	39.5±1.9	40.2±1.1	23.9±1.1	65.8±5.1	60.4±2.5	50.6±4.1
SCAN [40]	81.8±0.3	71.2±0.4	66.5±0.4	42.2±3.0	44.1±1.0	26.7±1.3	75.5±2.0	65.4±1.2	59.0±1.6
two-stage CRLC	84.2±0.1	74.7±0.3	70.6±0.5	45.0±0.7	44.8±0.8	28.7±0.9	78.7±1.1	68.4±1.6	62.7±1.8

Table 7: Two-stage clustering results on CIFAR10/20 and STL10.

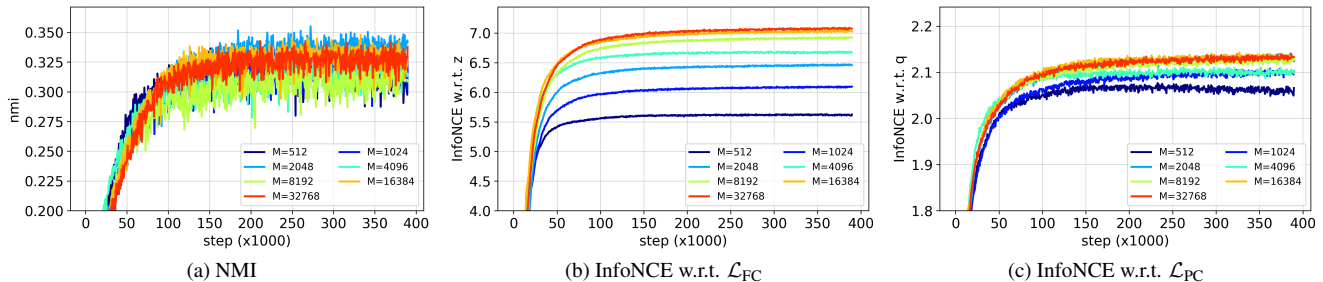


Figure 7: Learning curves of MemoryBank-based CRLC on CIFAR20 w.r.t. different numbers of negative samples. The momentum is $\alpha = 0.5$. The InfoNCE w.r.t. a contrastive loss is computed by using Eq. 2 in the main text.

is that for CIFAR10 and CIFAR20, the training set is big enough to cover the data distribution in the test set while for STL10, it does not apply (Table 4). Therefore, we think subsequent works should use only the training set when doing experiments on CIFAR10 and CIFAR20.

A.9. Additional two-stage clustering results

Table 7 compares the clustering results of “two-stage” CRLC and SCAN on CIFAR10/20, STL10. “Two-stage” CRLC clearly outperforms SCAN on all datasets.

A.10. Additional ablation study results

A.10.1 Contribution of the feature contrastive loss

In Fig. 6, we show the performance of CRLC on ImageNet-Dogs w.r.t. different coefficients of \mathcal{L}_{FC} (λ_2 in Eq. 11 in the main text). We observe that CRLC achieves the best clustering accuracy when $\lambda_2 = 3$. However, in Table 1 in the main text, we still report the result when $\lambda_2 = 10$.

A.10.2 Nonparametric implementation of CRLC

In this section, we empirically investigate the contributions of the number of negative samples and the momentum coefficient (α in Eq. 10 in the main text) to the performance of MemoryBank-based CRLC.

Contribution of the number of negative samples From Fig. 7a, we do not see any correlation between the number of negative samples and the clustering performance of MemoryBank-based CRLC despite the fact that increasing

the number of negative samples allows the RL-head and the C-head to gain more information from data (Figs. 7b and 7c). It suggests that for clustering (and possibly other classification tasks), getting more information may not lead to good results. Instead, we need to extract the right information related to clusters.

Contribution of the momentum coefficient From Fig. 8b, we see that changing the momentum value for updating probability vectors stored in the memory bank does not affect amount of information captured by the RL-head much. By contrast, in Fig. 8c, we see that larger values of the momentum cause the C-head to capture more information. This is reasonable because the accumulated probability vector $q_{n,t}$ is usually more stochastic (contains more information) than the probability vector \hat{q}_n of a particular view (Eq. 10 in the main text). Larger values of the momentum also cause the model to converge slower but do not affect the performance much (Fig. 8a).

A.11. Qualitative evaluation

In Fig. 9, we show the top correctly predicted samples according to their confidence score for each of 5 classes from the training set of STL10. It is clear that these samples are representative of the cluster they belong to.

A.12. Consistency-regularization-based semi-supervised learning methods

When some labeled data are given, the clustering problem naturally becomes semi-supervised learning (SSL).

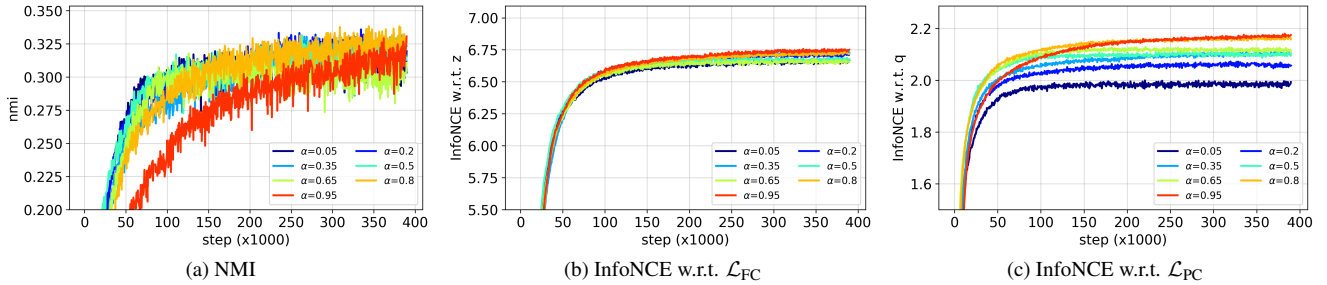


Figure 8: Learning curves of MemoryBank-based CRLC on CIFAR20 w.r.t. different values of the momentum. The number of negative samples is $M = 4096$. The InfoNCE w.r.t. a contrastive loss is computed by using Eq. 2 in the main text.

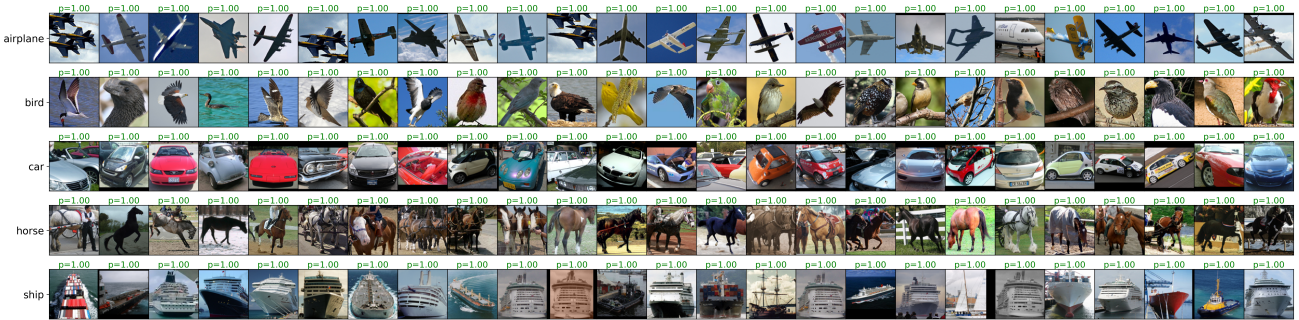


Figure 9: STL10 samples of 5 classes correctly predicted by CRLC. Samples are sorted by their confidence scores.

The core idea behind recent state-of-the-art SSL methods such as UDA [45], MixMatch [3], ReMixMatch [2], FixMatch [36] is *consistency regularization* (CR) which is about forcing an input sample under different perturbations/augmentations to have similar class predictions. In this sense, CR can be seen as an unnormalized version of the probability contrastive loss without the denominator. Different SSL methods extend CR in different ways. For example, UDA uses strong data augmentation to generate positive pairs. MixMatch and ReMixMatch combines CR with MixUp [52]. However, none of the above methods achieve consistent performance with extremely few labeled data (Section 5.2 in the main text). By contrast, clustering methods like CRLC perform consistently well even when no label is available. Thus, we believe designing a method that enjoys the strength of both fields is possible and CRLC-semi can be one step towards that goal.

A.13. Training setups for semi-supervised learning

To train CRLC-semi, we use a SGD optimizer with an initial learning rate = 0.1, momentum = 0.9, Nesterov = False, and weight decay = 5e-4. Similar to [36], we adjust the learning rate at each epoch using a cosine decay schedule [28] computed as follows:

$$lr_t = lr_{\min} + (lr_{\text{init}} - lr_{\min}) \times \frac{1 + \cos\left(\frac{t}{T}\pi\right)}{2}$$

where $lr_{\text{init}} = 0.1$, $lr_{\min} = 0.001$, lr_t is the learning rate at epoch t over T epochs in total. T is 2000 and 1000 for CIFAR10 and CIFAR100, respectively. The number of labeled and unlabeled samples in each batch is 64 and 512, respectively. In $\mathcal{L}_{\text{CRLC-semi}}$ (Eq. 12 in the main text), $\lambda_1 = 1$, $\lambda_2 = 5$, and $\lambda_3 = 1$.

We reimplement FixMatch using sample code from Github⁶ with the default settings unchanged. In this code, the number of labeled and unlabeled data in a batch is 64 and 448, respectively. However, the number of steps in one epoch does not depend on the batch size but is fixed at 1024. Thus, FixMatch is trained in 1024 epochs ≈ 1 million steps for both CIFAR10 and CIFAR100. Meanwhile, CLRC-semi is trained in only 194,000 steps for CIFAR10 and 97,000 steps for CIFAR100.

A.14. More results on semi-supervised learning

In Table 8, we show additional semi-supervised learning results of CRLC-semi on CIFAR10 and CIFAR100 in comparison with more baselines. CRLC-semi clearly outperforms all standard baselines like Π -model, Pseudo Labeling or Mean Teacher. However, CRLC-semi loses its advantage over holistic methods like MixMatch [3] and methods that use strong data augmentation like UDA [45] or ReMixMatch [2] when the number of labeled data is big

⁶<https://github.com/CoinCheung/fixmatch-pytorch>

Dataset	CIFAR10				CIFAR100			
	Labels	10	20	40	250	100	200	400
PI-model [24]	-	-	-	54.26±3.97	-	-	-	57.25±0.48
Pseudo Labeling [25]	-	-	-	49.78±0.43	-	-	-	57.38±0.46
Mean Teacher [38]	-	-	-	32.32±2.30	-	-	-	53.91±0.57
MixMatch [3]	-	-	47.54±11.50	11.05±0.86	-	-	67.61±1.32	39.94±0.37
UDA [45]	-	-	29.05±5.93	8.82±1.08	-	-	59.28±0.88	33.13±0.22
ReMixMatch [2]	-	-	19.10±9.64	5.44±0.05	-	-	44.28±2.06	27.43±0.31
FixMatch (RA) [36]	-	-	13.81±3.37	5.07±0.65	-	-	48.85±1.75	28.29±0.11
ReMixMatch ^{†7}	59.86±9.34	41.68±8.15	28.31±6.72	-	76.32±4.30	66.51±2.86	52.23±1.71	-
FixMatch (RA) ^{†8}	25.49±7.74	21.15±8.96	8.87±4.29	-	79.27±2.65	68.58±0.7	57.52±1.5	-
CRLC-semi	46.75±8.01	29.81±1.18	19.87±0.82	13.53±0.21	82.20±1.15	73.04±1.15	60.87±0.17	41.10±0.12

Table 8: Full classification errors on CIFAR10 and CIFAR100. Lower values are better. Results of baselines are taken from [36]. †: Results obtained from external implementations of models.

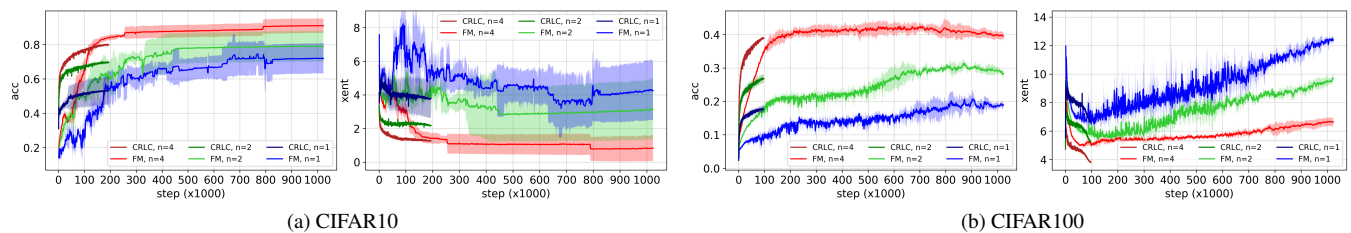


Figure 10: Test accuracy and crossentropy curves of CRLC-semi (CRLC) and FixMatch (FM) on CIFAR10 and CIFAR100 with 1, 2, 4 labeled samples per class. It is clear that CRLC-semi performs consistently in all cases except for the case of CIFAR10 with 1 labeled sample per class. However, even in that case, the CRLC-semi still gives consistent performance for each run (Fig. 11). FixMatch, by contrast, is very inconsistent in its performance for each run, especially on CIFAR10.

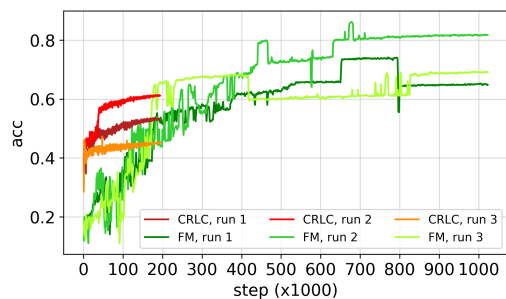


Figure 11: Test accuracy curves of CRLC-semi (CRLC) and FixMatch (FM) on CIFAR10 with 1 labeled samples per class w.r.t. 3 different runs.

enough. Currently, we are not sure whether the problem comes from the feature contrastive loss \mathcal{L}_{FC} (when we have enough labels, representation learning may act as a regularization term and reduce the classification result), or from the negative entropy term in $\mathcal{L}_{cluster}$ (causing too much regularization), or even from the probability contrastive loss (contrasting probabilities of two related views is not suit-

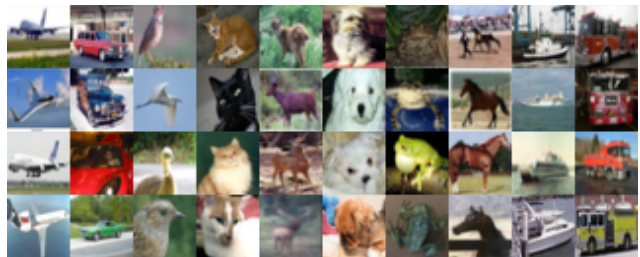


Figure 12: 40 labeled CIFAR10 samples organized into 4 rows where each row has 10 images corresponding to 10 classes. For 10 and 20 labeled samples, the first row and the first two rows are considered, respectively.

```
[[33797 42143 20308 23202 39495 37706 17788 22128 38925 5884]
 [ 2804 39911 6041 11188 20588 33193 16982 15878 42066 27972]
 [19066 2339 24978 1098 12132 15219 14139 2358 40495 37444]
 [19065 19165 16050 31194 3377 26529 22764 7989 14979 43282]]
```

Figure 13: Indices in the training set of the images in Fig. 12

able when we have enough labels). Thus, we leave the answer of this question for future work. To gain more insight

about the advantages of our proposed CRLC-semi, we provide detailed comparison between this method and the best SSL baseline - FixMatch [36] in the next section.

Direct comparison between CRLC-semi and FixMatch

FixMatch [36] is a powerful SSL method that makes use of pseudo-labeling [25] and strong data augmentation [10] to generate quality pseudo-labels for training. FixMatch has been shown to work reasonably well with only 1 labeled sample per class. In our experiment, we observe that FixMatch outperforms CRLC-semi on both CIFAR10 and CIFAR100. However, FixMatch must be trained in much more steps than CRLC-semi to achieve good results and its performance is very inconsistent (like other SSL baselines) compared to that of CRLC-semi (Figs. 10, 11).

Details of the labeled samples For the purpose of comparison and reproducing the results in Table 8, we provide the indices of 40 labeled CIFAR10 samples and 400 labeled CIFAR100 samples used in our experiments in Fig. 13 and Fig. 15, respectively. We also visualize these samples in Fig. 12 and 14. We note that we do not cherry-pick these samples but randomly draw them from the training set.

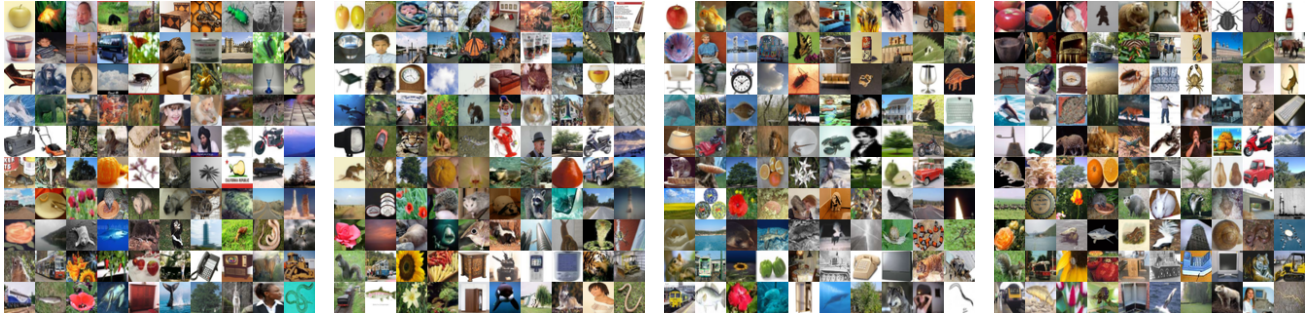


Figure 14: 400 labeled CIFAR100 samples organized into 4 image blocks where each image block is a set of 100 images corresponding to 100 classes. For 100 and 200 labeled samples, the first block and the first two blocks are considered, respectively.

Block 1	Block 2
[11188 12218 6223 32575 15073 31887 46913 24978 26529 14442]	[39404 41352 37487 21791 24545 33045 39512 35960 33548 35465]
[29329 38925 42143 9627 17117 26223 49586 15463 14283 21116]	[32244 22764 42462 11395 10836 14064 20797 15878 37129 8097]
[14139 9544 25304 44940 23202 49718 3328 1538 42066 19066]	[42221 47066 46915 1788 11672 41659 35411 42141 46765 3788]
[35592 39911 26534 47536 5884 28737 31867 10818 2363 24205]	[11894 21483 21743 16576 30846 39504 43770 26677 47042 49729]
[48129 14360 2339 30952 19165 16982 39711 39354 41086 10609]	[23392 2732 16269 22389 47738 32627 4859 49852 20985 34982]
[17925 6041 17788 40459 14979 11003 25059 49750 20308 38061]	[4885 12132 11095 29010 6592 28341 15536 38534 37706 10927]
[1335 13367 27767 33797 19065 17978 46845 1088 3377 24528]	[3388 43257 8092 44052 7783 8225 9025 25138 25540 34907]
[37444 13803 15977 4794 15219 39495 31626 48985 12344 20588]	[29427 36540 17999 18832 8423 1045 44302 37176 5845 24493]
[45896 35097 31194 48299 27972 40517 23900 45209 3336 33193]	[25850 24481 43866 42061 42445 30962 2235 42427 17239 1791]
[43282 37265 40495 46028 16050 8935 38158 43907 8983 24193]	[32694 48503 2804 26725 20441 42567 48444 37047 26901 13813]
Block 3	Block 4
[36391 42934 35048 13579 8292 45480 42748 45984 11381 46018]	[30442 39988 32270 6709 7017 26062 47575 20284 20982 31699]
[25501 35130 22658 5243 4287 32594 38519 7989 36761 4356]	[29045 14242 36386 18365 35688 19535 39851 3473 15969 35477]
[25513 28523 7341 26116 10648 16563 20562 9467 42004 35726]	[2653 44887 37250 45939 27313 5377 7564 35108 38461 2881]
[46746 21177 42454 15881 26838 24142 47376 8800 34485 33238]	[24036 19749 16007 30737 2324 21277 38917 40713 25945 33506]
[12220 1216 34677 15429 35645 34202 43344 14026 1170 34224]	[3671 41641 16667 30119 30028 19345 15737 5637 44468 24588]
[27277 1098 27 30163 48136 31554 36374 13139 21529 4708]	[32841 22128 37091 20991 10893 47385 38346 3399 3159 18757]
[21360 11965 1695 37345 3968 36877 2358 34036 45044 31733]	[14970 46469 4780 26897 31836 31718 15863 2906 48034 19203]
[45776 48496 34381 44941 8407 47812 11034 43694 47371 21209]	[5679 30322 39035 28835 21763 39729 28298 46213 32227 4517]
[13998 43513 39228 3563 44723 16640 38753 16465 38529 40484]	[28894 22504 19817 27575 37802 31236 5186 29915 39333 5896]
[26700 39133 36219 31865 49277 46387 19415 17068 26761 14239]	[37311 11193 32734 42035 10314 4613 34299 26479 3272 41338]

Figure 15: Indices in the training set of the images in Fig. 14